Supporting Information

Wang et al. 10.1073/pnas.1417923111

SI Materials and Methods

A. ^{13}C NMR Experiments. KSI^{D40N} labeled with $^{13}C_\zeta$-tyrosine was concentrated to ~1 mM in 40 mM potassium phosphate buffer (pH 7.2) and loaded into a Shigemi tube. NMR spectra were acquired at 25 °C on a 500-MHz (proton frequency) Varian INOVA spectrometer. 1D free induction decays were acquired with proton decoupling and 2-s recycle delays, processed with a 10-Hz line-broadening function, and referenced against the upfield carbon peak of sodium 3-trimethylsilyl-propionate-2,2,3,3-d_4 (0 ppm), similar to previous reports (1, 2). For spectra in H_2O, the buffer consisted of a small portion of D_2O as lock solvent (5%, vol/vol). For the D_2O samples, the solvent was 100% (vol/vol) D_2O. The ^{13}C NMR spectra are shown in Fig. S4.

B. Estimates of the Fractional Ionizations from ^{13}C NMR. Previous work has shown that the ^{13}C chemical shift of the ζ-carbon of tyrosine (analogously, C-1 of phenol) is sensitive to the ionization state of the adjacent hydroxyl group (3), shifting 10.8 ppm downfield on transitioning from a fully protonated (pH 2; 155.5 ppm) to a fully ionized (pH 14; 166.3 ppm) form. Based on these observations, we have used the chemical shifts of the assigned $^{13}C_\zeta$ peaks (1) to estimate the fractional ionizations ($\%I$) of the three tyrosines in the triad. The conversion between chemical shift and fractional ionization is achieved using the equation

$$\%I_{raw} = \left(\delta_{apo} - \delta_{ref}\right) / \left(166 - \delta_{ref}\right), \qquad \textbf{[S1]}$$

in which δ_{apo} is the chemical shift of one of the tyrosines (either Tyr16, Tyr32, or Tyr57) in Fig. S4*A* (Table S3), δ_{ref} is the chemical shift of the same tyrosine in a reference system in which the tyrosines are fully protonated (2), and 166 ppm is an estimate for the chemical shift of a fully ionized tyrosine. Eq. **S1** assumes a linear relationship between fractional ionization and chemical shift over the full dynamic range, which implies fast proton transfer on the NMR chemical shift timescale. This assumption seems to be valid in previous work (2, 4) and is additionally supported by the simulations presented here. Eq. **S1** also makes a more drastic assumption that changes in chemical shift can be fully attributed to changes in fractional ionization—that is, it neglects the dependence of the chemical shift on the local environment and the isotopic composition of the molecule. We, therefore, must regard the values of fractional ionization that are derived to be estimates, although both of these assumptions find some validity by comparing data found on KSI^{D40N} (Fig. S4*A*) with those of WT KSI (Fig. S4*B*) vide infra.

The fractional ionizations that arise from applying Eq. **S1** ($\%I_{raw}$) do not sum to unity (Table S3). The origin of this feature is likely because of the contribution of the KSI active-site environment, which could make the basis chemical shift for fully ionized TyrX different from that of tyrosine in solution (166 ppm). Importantly, however, the sum of the raw fractional ionizations is quite similar for the two isotopomers, suggesting that the environment effects are constant between the two isotopomers and therefore, would cancel when we calculate the change in fractional ionization on isotopic replacement ($\Delta\%I$).

We normalized the fractional ionizations by treating them with a uniform arithmetic correction:

$$\%I_{norm} = \%I_{raw} - (\Sigma\%I_{raw} - 100)/3, \qquad \textbf{[S2]}$$

which assumes that each of the three tyrosines would have the same chemical shift if it were fully ionized. This assumption is at least supported by the observation that three tyrosines have relatively similar chemical shifts when they are fully neutral, such as in WT KSI (Fig. S4*B*). Nevertheless, we caution that, because this normalization scheme is not perfect, the values reported for $\Delta\%I$ are more reliable that the absolute $\%I$ values.

The structure of WT KSI is nearly identical to that of KSI^{D40N} (including the environment around the tyrosine cluster), but in WT KSI, none of the tyrosines are ionized. On isotopic replacement, all of the resonances shift upfield by 120 ± 15 ppb, likely reflecting the intrinsic effect of isotopic composition on chemical shift. However, the shifts on isotopic replacement in KSI^{D40N} are substantially more varied and larger, suggesting that the majority of this effect cannot be merely caused by the isotopic composition itself but rather, the changes in fractional ionization that accompany it.

C. $\Delta\Delta pK_a$ Calculations. The pK_a change on H/D substitution (ΔpK_a) for KSI and tyrosine in aqueous solution can be calculated from the free-energy changes (ΔA):

$$\Delta pK_a^{KSI} = pK_a^{KSID} - pK_a^{KSIH} = \frac{\Delta A_2 - \Delta A_1}{2.303 k_B T} = \frac{\Delta A_{KSIH} - \Delta A_{KSI-} - \Delta A_H}{2.303 k_B T}$$

and

$$\Delta pK_a^{Sol} = pK_a^{TyrD} - pK_a^{TyrH} = \frac{\Delta A_4 - \Delta A_3}{2.303 k_B T} = \frac{\Delta A_{TyrH} - \Delta A_H}{2.303 k_B T}$$

for the following thermodynamic cycles:

$$\begin{array}{ccccccc} \mathrm{KSIH} & \rightleftharpoons & \mathrm{KSI^-} & + & \mathrm{H^+} & \Delta A_1 \\ \Delta A_{\mathrm{KSIH}}\uparrow & & \uparrow\Delta A_{\mathrm{KSI-}} & & \uparrow\Delta A_{\mathrm{H}} & \\ \mathrm{KSID} & \rightleftharpoons & \mathrm{KSID^-} & + & \mathrm{D^+} & \Delta A_2 \\ \mathrm{TyrH} & \rightleftharpoons & \mathrm{Tyr^-} & + & \mathrm{H^+} & \Delta A_3 \\ \Delta A_{\mathrm{TyrH}}\uparrow & & & & \uparrow\Delta A_{\mathrm{H}} & \\ \mathrm{TyrD} & \rightleftharpoons & \mathrm{Tyr^-} & + & \mathrm{D^+} & \Delta A_4. \end{array}$$

Here, KSIH and KSI$^-$ denote KSI^{D40N} with the side-chain phenol group of Tyr57 neutral or ionized, respectively. KSID represents KSI^{D40N} with a neutral Tyr57 and H16, H32, and H57 replaced by D. Likewise, KSID$^-$ has an ionized Tyr57, with H16 and H32 being substituted by D. Tyr$^-$ represents tyrosine in aqueous solution with the side-chain group ionized. TyrD denotes tyrosine in aqueous solution with the side-chain O–H group being replaced by O–D.

We calculated the excess isotope effects on the pK_a ($\Delta\Delta pK_a$), which is a probe of the quantum effects caused by the enzyme environment that is not present in aqueous solution. In addition, because $\Delta\Delta pK_a$ naturally cancels the solvent contribution to ΔpK_a (see the above cycle), it significantly reduces the computational cost.

From the thermodynamic cycles, $\Delta\Delta pK_a$ is

$$\Delta\Delta pK_a \equiv \Delta pK_a^{KSI} - \Delta pK_a^{Sol} = \frac{\Delta A_{KSIH} - \Delta A_{KSI-} - \Delta A_{TyrH}}{2.303 k_B T}.$$

In the above equation, the ΔA values are free-energy changes upon converting D to H in a given system i and can be calculated

from the quantum kinetic energies of the hydrogen isotopes by (5, 6)

$$\Delta A_i = -\int_{m_D}^{m_H} d\mu \frac{\langle K_i(\mu)\rangle}{\mu}.$$

$K_i(\mu)$ is the quantum kinetic energy of a hydrogen isotope of mass μ. The quantum kinetic energy of H can be calculated directly from AI-PIMD simulations using the centroid virial estimator (7, 8), and $K_i(\mu)$ was obtained using the thermodynamic free-energy perturbation path integral estimator (5). Simulations of $KSID^-$ and KSID were performed, and the resulting $K_i(m_D)$ values were within the error bars of those obtained from the thermodynamic free-energy perturbation estimator.

D. Model Tyrosine Triad Calculations of Proton-Sharing Energy, $\Delta E_{\nu=0}$. To investigate the effect of the O–O distance between O16 and O57 on the energy required to share a proton between residues ($\Delta E_{\nu=0}$), we constructed a model of the tyrosine triad where we could systematically change the O–O distance. This model consisted of the *p*-methylene phenol side chains of residues Tyr16, Tyr32, and Tyr57, with the side chain of Tyr57 ionized. The heavy-atom positions of the tyrosine triad were taken from the Protein Data Bank ID code 1OGX (9) crystal structure of KSI^{D40N}. Because the crystal structure does not contain hydrogen atom information, hydrogen atoms were added, and their positions were optimized by energy minimization at the B3LYP-D3 level. The termini of the side chains were capped with hydrogen atoms. The resulting atoms included in the triad were, thus, identical to the QM region in the AI-PIMD simulations of KSI^{D40N} with ionized Tyr57 (Fig. S5*A*). However, in contrast to our AI-PIMD simulations, the protein environment was not included in these model calculations. Removal of the protein environment allowed us to move the tyrosine residues relative to each other to obtain values for $\Delta E_{\nu=0}$ at different O–O distances without creating overlaps with the rest of the protein.

To obtain $\Delta E_{\nu=0}$ as a function of the O57–O16 distance, Tyr32 and Tyr57 were fixed in space, and Tyr16 was translated along the O57–O16 vector. At each O–O distance, a proton scan was carried out by calculating the potential energy associated with moving the proton along the O57–O16 vector with all other coordinates held fixed. $\Delta E_{\nu=0}$ was obtained by taking the difference between potential energy at $\nu = 0$ and the lowest value of the energy obtained along the scan.

The electronic structure calculations were performed using the B3LYP functional (10) with D3 dispersion corrections (11) and the 6–31G* basis set using the TeraChem software (12).

1. Schwans JP, Sunden F, Gonzalez A, Tsai Y, Herschlag D (2013) Uncovering the determinants of a highly perturbed tyrosine pK_a in the active site of ketosteroid isomerase. *Biochemistry* 52(44):7840–7855.
2. Sigala PA, et al. (2013) Quantitative dissection of hydrogen bond-mediated proton transfer in the ketosteroid isomerase active site. *Proc Natl Acad Sci USA* 110(28): E2552–E2561.
3. Fafarman AT, et al. (2012) Quantitative, directional measurement of electric field heterogeneity in the active site of ketosteroid isomerase. *Proc Natl Acad Sci USA* 109(6):E299–E308.
4. Fried SD, Boxer SG (2012) Evaluation of the energetics of the concerted acid-base mechanism in enzymatic catalysis: The case of ketosteroid isomerase. *J Phys Chem B* 116(1):690–697.
5. Ceriotti M, Markland TE (2013) Efficient methods and practical guidelines for simulating isotope effects. *J Chem Phys* 138(1):014112.
6. Wang L, Ceriotti M, Markland TE (2014) Quantum fluctuations and isotope effects in ab initio descriptions of water. *J Chem Phys* 141(10):104502.
7. Cao J, Berne BJ (1989) On energy estimators in path integral Monte Carlo simulations: Dependence of accuracy on algorithm. *J Chem Phys* 91(10):6359–6366.
8. Herman MF, Bruskin EJ, Berne BJ (1982) On path integral Monte Carlo simulations. *J Chem Phys* 76(10):5150–5155.
9. Ha N-C, Kim M-S, Lee W, Choi KY, Oh B-H (2000) Detection of large pK_a perturbations of an inhibitor and a catalytic group at an enzyme active site, a mechanistic basis for catalytic power of many enzymes. *J Biol Chem* 275(52):41100–41106.
10. Becke AD (1993) Density-functional thermochemistry. III. The role of exact exchange. *J Chem Phys* 98(7):5648–5652.
11. Grimme S, Antony J, Ehrlich S, Krieg H (2010) A consistent and accurate ab initio parameterization of density functional dispersion correction (DFT-D) for the 94 elements H-Pu. *J Chem Phys* 132(15):154104.
12. Ufimtsev IS, Martinez TJ (2009) Quantum chemistry on graphical processing units. 3. Analytical energy gradients, geometry optimization, and first principles molecular dynamics. *J Chem Theory Comput* 5(10):2619–2628.

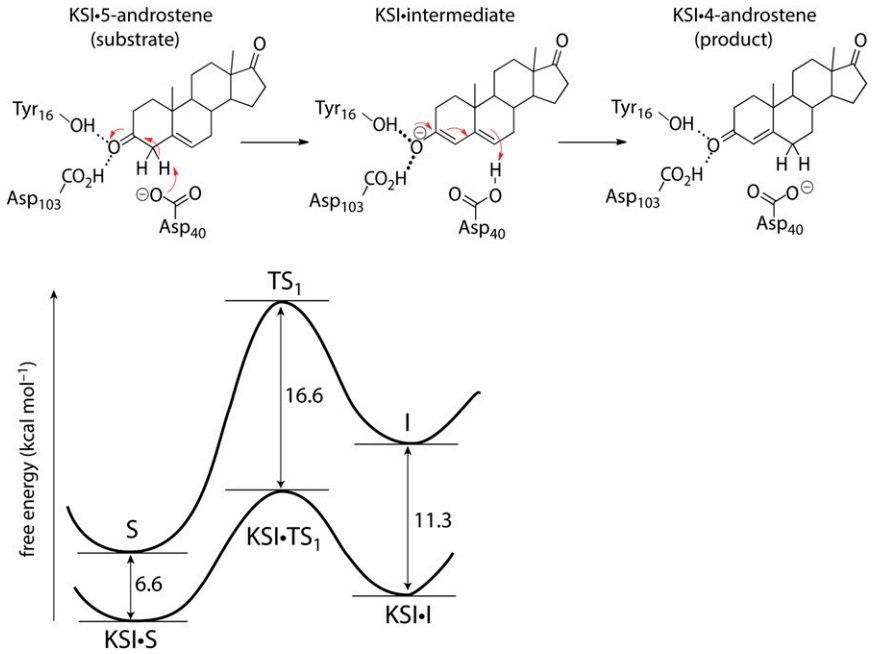

Fig. S1. Consensus mechanism of KSI. KSI rapidly converts 5-androstene to 4-androstene in two steps. The α-proton adjacent to the carbonyl is abstracted using the Asp40 general base to form an enzyme-bound dienolate intermediate. The intermediate is stabilized by 11.3 kcal/mol by accepting two direct hydrogen bonds from Tyr16 and Asp103. The proton on Asp40 is returned to the steroid two carbons away to form a conjugated ketone product. The reaction profile diagram illustrates the relative energetics between the above chemical reaction when it is catalyzed by (lower trace) KSI or (upper trace) acetate in solution. Stabilization of substrate and intermediate is based on binding constants; stabilization of the transition state (TS) is based on the ratio of rate constants.

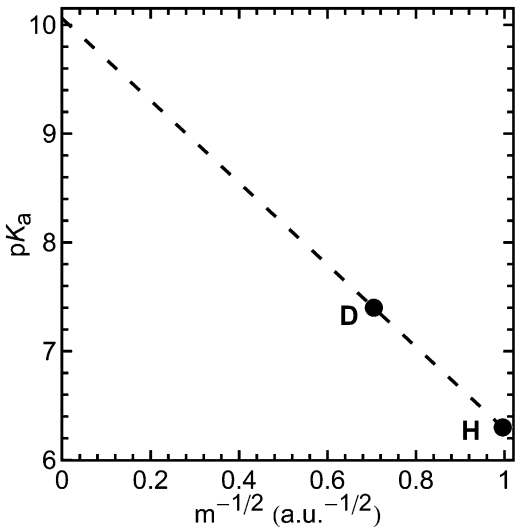

Fig. S2. Extrapolation of pK_a to classical limit. Experimental pK_a values of Tyr57 in H_2O and D_2O are shown as black dots. In the quasiharmonic limit, pK_a scales linearly with respect to the inverse square root of the hydrogen isotope mass (dotted line). The masses are in atomic units. The extrapolation to the classical limit ($m\rightarrow\infty$) yields a pK_a value of 10.1 $\pm$ 0.5 for Tyr57.

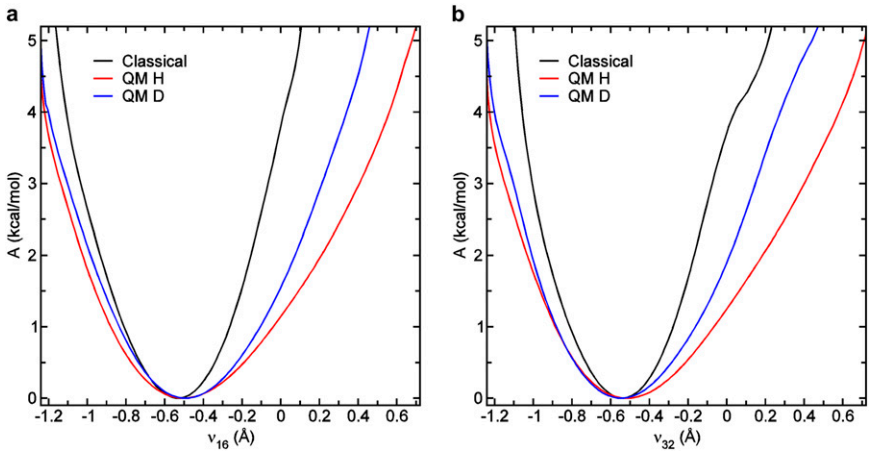

Fig. S3. Free-energy surface along the proton transfer coordinate ν. Free energy A as a function of the proton transfer coordinates (*A*) ν_{16} and (*B*) ν_{32} when the nuclei are treated classically (Classical) or quantum mechanically for H (QM H) and D (QM D).

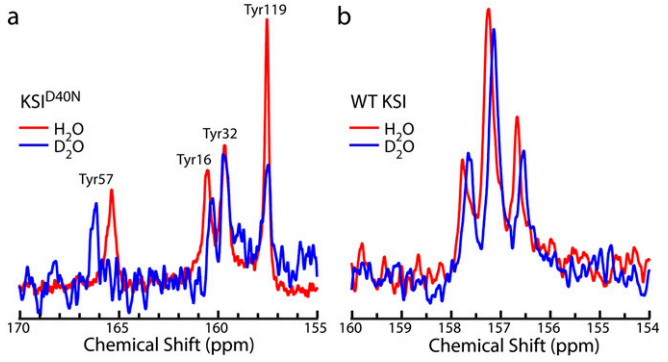

Fig. S4. Chemical shift isotope effects. ^{13}C NMR spectra of $^{13}C_\varepsilon$-Tyr–labeled KSI (*A*) with and (*B*) without the Asp40Asn mutation. Traces in red are in H_2O (5% D_2O for locking), and traces in blue are in 100% D_2O. Assignments of the peaks are shown for KSI^{D40N}. Table S3 shows fractional ionizations.

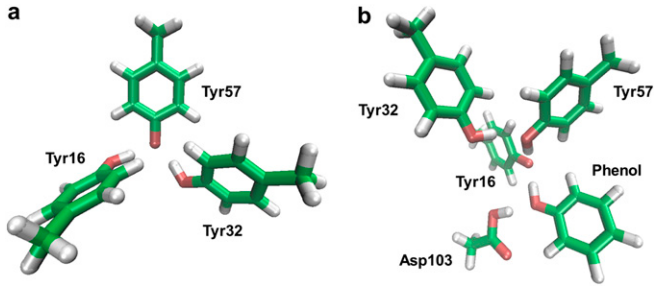

Fig. S5. QM regions used in simulations. Snapshot of the QM regions of (*A*) KSI^{D40N} with ionized Tyr57 (shown in the orientation in Fig. 3) and (*B*) KSI^{D40N} with the bound phenol (shown in the orientation in Fig. 5). Hydrogen capping atoms are also shown. Green, red, and white represent C, O, and H atoms, respectively.

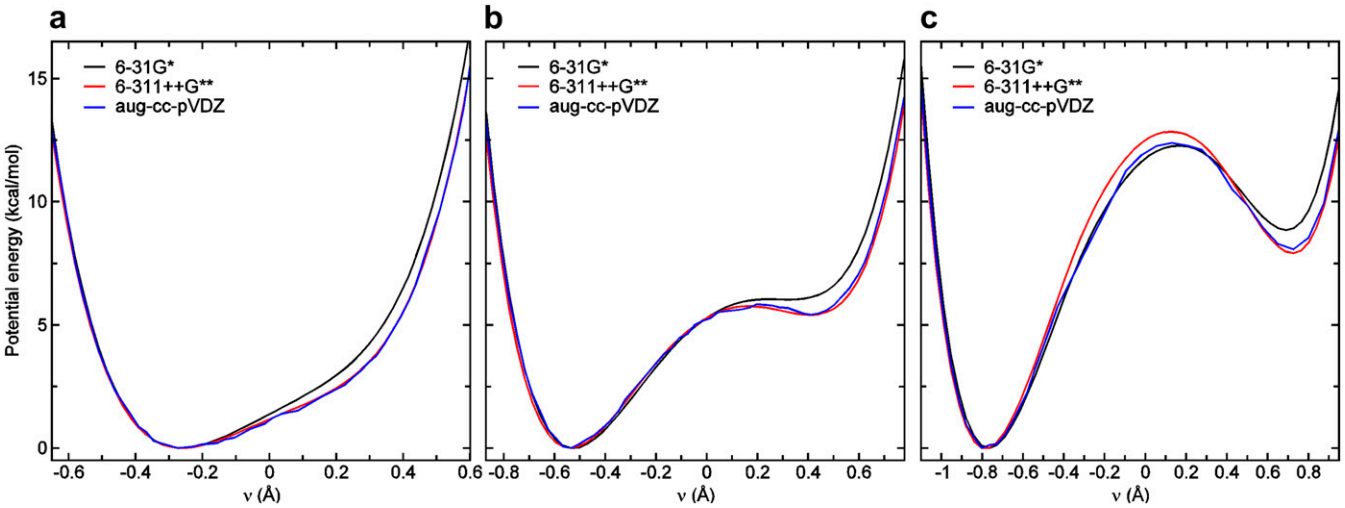

Fig. S6. Potential energy profiles showing basis set convergence. Potential energy as a function of the proton transfer coordinate ν for O–O distances of (*A*) 2.4, (*B*) 2.6, and (*C*) 2.8 Å. The electronic structure calculations were performed on the model tyrosine triad (*SI Materials and Methods*, section D) using the B3LYP functional (1) with the D3 correction (2) and the 6–31G*, 6–311++G**, and aug-cc-pVDZ basis sets. The 6–31G* basis set reproduces the potential energy profiles of the large basis sets with a maximum error of 0.9 kcal/mol and a mean absolute error of 0.4 kcal/mol in all thermally relevant regions.

1. Becke AD (1993) Density-functional thermochemistry. III. The role of exact exchange. *J Chem Phys* 98(7):5648–5652.
2. Grimme S, Antony J, Ehrlich S, Krieg H (2010) A consistent and accurate ab initio parameterization of density functional dispersion correction (DFT-D) for the 94 elements H-Pu. *J Chem Phys* 132(15):154104.

Table S1. Experimental acid dissociation constants of tyrosine and KSI^{D40N} as measured by monitoring changes in absorption at 300 nm as a function of *pL* (where *L* = H or D)

Species and solvent	pK_a^*	ΔpK_a	$\Delta\Delta pK_a$
Tyrosine			
H_2O	10.24 ± 0.07	0.53 ± 0.08	
D_2O	10.77 ± 0.04		
KSI^{D40N}			0.57 ± 0.16
H_2O	6.3 ± 0.1	1.1 ± 0.14	
D_2O	7.4 ± 0.1		

Error bars are the random errors from multiple replicates, and they are propagated accordingly.
*Absolute pK_a values are subject to (sometimes significant) systematic error in the pH electrode, although this error will cancel when determining pK_a differences.

Table S2. Summary of the number of atoms in the QM and MM regions of the AI-PIMD simulations

Simulation	QM atoms	MM atoms
KSI^{D40N} with ionized Tyr57	47	56,504
KSI^{D40N} with neutral Tyr57	48	56,504
KSI^{D40N} with bound phenol	68	52,204
Tyrosine in aqueous solution	139	5,037

Table S3. ^{13}C NMR data and determination of fractional ionizations (%*I*)

		KSI^{D40N} (H_2O)			KSI^{D40N} (D_2O)			
Residue	Ref. (δ/ppm)	δ/ppm	%*I* (raw)	%*I* (norm)	δ/ppm	%*I* (raw)	%*I* (norm)	Δ%*I* (H→D)
Tyr16	158.54	160.52	26.5	13	160.26	23.0	8	−5
Tyr32	157.97	159.66	21.0	8	159.73	21.9	6	−2
Tyr57	157.97	165.36	92.0	79	166.13	101	86	+7
Total			139.5	100		145.9	100	

Chemical shifts extracted from 1D ^{13}C NMR spectra of KSI^{D40N}, in which only the ζ-carbon of tyrosine residues is enriched in ^{13}C. Fractional ionizations (%*I*) were determined using methods described in *SI Materials and Methods*, section B (1). The reference chemical shifts refer to the chemical shifts of a complex of KSI^{D40N} and 4-nitrophenol, in which the phenol is 100% ionized and the tyrosines are believed to be 0% ionized.

1. Sigala PA, et al. (2013) Quantitative dissection of hydrogen bond-mediated proton transfer in the ketosteroid isomerase active site. *Proc Natl Acad Sci USA* 110(28):E2552–E2561.

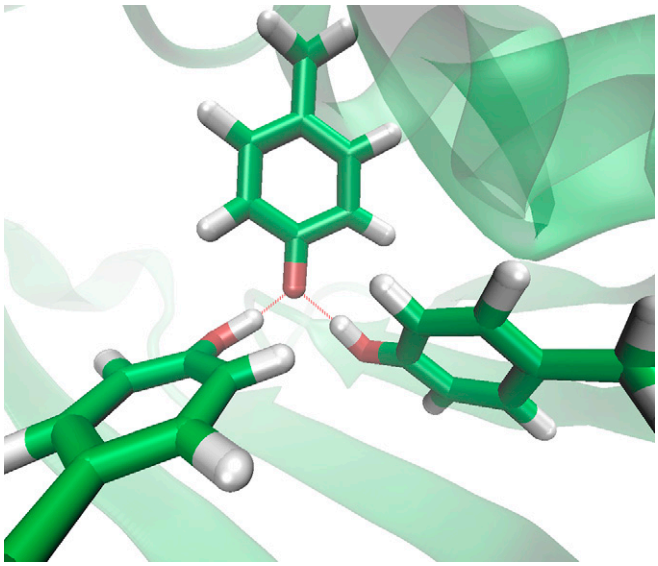

Movie S1. Trajectory of KSI^{D40N} with ionized Tyr57 from the classical AIMD simulation. H16 and H32 remain bonded to their respective oxygens throughout the simulation. Green, red, and white represent carbon, oxygen, and hydrogen atoms, respectively. The three residues shown are (*Left*) Tyr16, (*Right*) Tyr32, and (*Upper*) Tyr57. The protein environment in the MM region is also included.

Movie S1

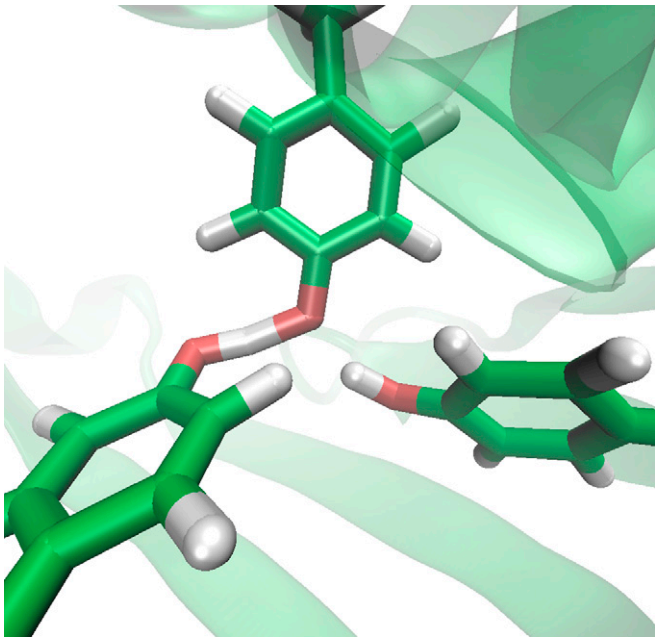

Movie S2. Trajectory of KSI^{D40N} with ionized Tyr57 from the AI-PIMD simulation. Because the six path integral beads used in the simulation are equivalent, the trajectory is shown for one bead. Frequent proton transfer can be observed in the trajectory. Green, red, and white represent carbon, oxygen, and hydrogen atoms, respectively. The three residues shown are (*Left*) Tyr16, (*Right*) Tyr32, and (*Upper*) Tyr57. The protein environment is also included.

Movie S2

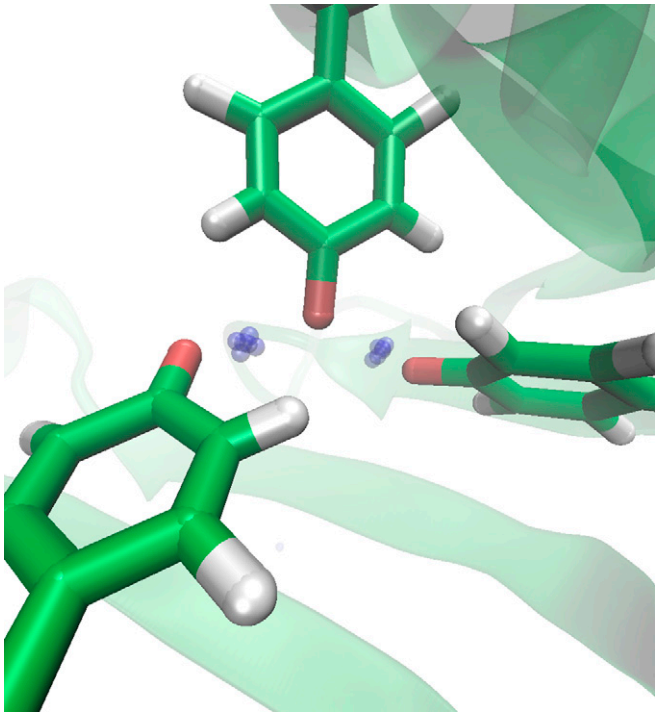

Movie S3. Trajectory of KSI^{D40N} with ionized Tyr57 from the AI-PIMD simulation. Protons H16 and H32 (shown as their full ring polymers) are delocalized between the hydrogen-bonded oxygens. Green, red, and white represent carbon, oxygen, and hydrogen atoms, respectively. The blue-gray circles represent position uncertainty of H16 and H32. For clarity, other atoms are shown as their centroids. The three residues shown are (*Left*) Tyr16, (*Right*) Tyr32, and (*Upper*) Tyr57. The protein environment is also included in the video.

Movie S3